Modulation of Locally Generated Equatorial Noise by ULF Wave

UT Dallas Author(s):

Hui Zhu
Lunjin Chen
Xu Liu

Citation:

Zhu, H., L. Chen, X. Liu, and Y. Y. Shprits. 2019. "Modulation of Locally Generated Equatorial Noise by ULF Wave." Journal Of Geophysical Research: Space Physics 124(4): 2779-2787, doi: 10.1029/2018JA026199

JGR Space Physics

RESEARCH ARTICLE
10.1029/2018JA026199

Modulation of Locally Generated Equatorial Noise by ULF Wave

Hui Zhu[1], Lunjin Chen[1], Xu Liu[1], and Yuri Y. Shprits[2,3,4]

[1]Department of Physics, University of Texas at Dallas, Richardson, TX, USA, [2]GFZ German Research Centre for Geosciences, Potsdam, Germany, [3]Institute of Physics and Astronomy, University of Potsdam, Potsdam, Germany, [4]Department of Earth and Planetary Space Sciences, University of California, Los Angeles, CA, USA

Key Points:
- The PSD of ring proton is antiphase modulated by ULF wave
- A rare and fortunate MS wave modulated by ULF wave is reported for the first time
- Linear theory and perpendicular propagation account for the modulation of MS

Correspondence to:
H. Zhu and L. Chen,
zhuhui328@gmail.com;
lunjin.chen@gmail.com

Citation:
Zhu, H., Chen, L., Liu, X., & Shprits, Y. Y. (2019). Modulation of locally generated equatorial noise by ULF wave. *Journal of Geophysical Research: Space Physics*, *124*, 2779–2787. https://doi.org/10.1029/2018JA026199

Received 15 OCT 2018
Accepted 7 APR 2019
Accepted article online 12 APR 2019
Published online 23 APR 2019

Abstract In this paper we report a rare and fortunate event of fast magnetosonic (MS, also called equatorial noise) waves modulated by compressional ultralow frequency (ULF) waves measured by Van Allen Probes. The characteristics of MS waves, ULF waves, proton distribution, and their potential correlations are analyzed. The results show that ULF waves can modulate the energetic ring proton distribution and in turn modulate the MS generation. Furthermore, the variation of MS intensities is attributed to not only ULF wave activities but also the variation of background parameters, for example, number density. The results confirm the opinion that MS waves are generated by proton ring distribution and propose a new modulation phenomenon.

1. Introduction

Fast magnetosonic (MS, also named equatorial noise) waves are an important type of electromagnetic emissions in the terrestrial magnetosphere, occurring over the frequency range between the proton gyrofrequency and the lower hybrid resonance frequency (Balikhin et al., 2015; Perraut et al., 1982; Santolík et al., 2002). MS waves are usually confined within a few degrees near the geomagnetic equator both inside and outside the plasmapause (Gurnett, 1976; Němec et al., 2005; Russell et al., 1970; Santolík et al., 2004). Both theoretical and observational studies (Boardsen et al., 1992; Chen, 2015; Chen et al., 2010; Curtis & Wu, 1979; Horne et al., 2000; Liu et al., 2011; Ma et al., 2014; Meredith et al., 2008) have suggested that the ring distribution ($\partial f/\partial v_\perp > 0$) of energetic protons at energies of several tens of kiloelectron volts can provide the free energy to excite the MS waves with highly oblique normal angels at discrete harmonics of proton gyrofrequency. In addition to the discrete nature the mechanism behind remains an open question. MS waves are believed to cause the local acceleration of radiation belt energetic electrons via Landau resonance (Horne et al., 2007; Ma et al., 2016; Shprits et al., 2013). Additional effects caused by MS waves such as transit time scattering (Bortnik & Thorne, 2010; Li et al., 2014) and bounce resonance (Chen et al., 2015; Li et al., 2015) are proposed. Recent studies (Liu et al., 2018; Yuan et al., 2017) show that the variation of background plasma environment (e.g., solar wind pressure and cold electron number density) significantly influences the appearance of MS wave, which have attracted much attention.

Ultralow frequency (ULF) waves could be driven by the external sources (e.g., solar wind activity) and internal sources (e.g., plasma instability; Hughes, 1994). ULF waves are able to directly scatter the radiation belt electrons via radial diffusion (Elkington et al., 1999; Fälthammar, 1965; Su et al., 2015) or indirectly modulate other scattering agents, such as very low frequency wave excitations, for example, chorus waves. W. Li et al. (2011) established statistically the roles of external-driven compressional Pc4–Pc5 pulsations in the modulation of chorus waves, and Xia et al. (2016) demonstrated a modulation event deep inside the magnetosphere, where internal-driven ULF waves modulated the electron pitch angle distribution and thus chorus wave generation. They both suggested that the anticorrelaton between magnetic fluctuation and density variation driven by ULF waves is responsible for the modulation of chorus generation. However, the potential role of ULF waves in the process of MS generation has not been confirmed yet because none of the studies have identified ULF waves that are responsible for MS instability in the generation region. In this study, we will report a rare and fortunate ULF-modulated MS wave event observed by Van Allen Probes (Mauk et al., 2013). The simultaneous ULF wave activity and proton distributions are analyzed in order to gain insight of modulation mechanism.

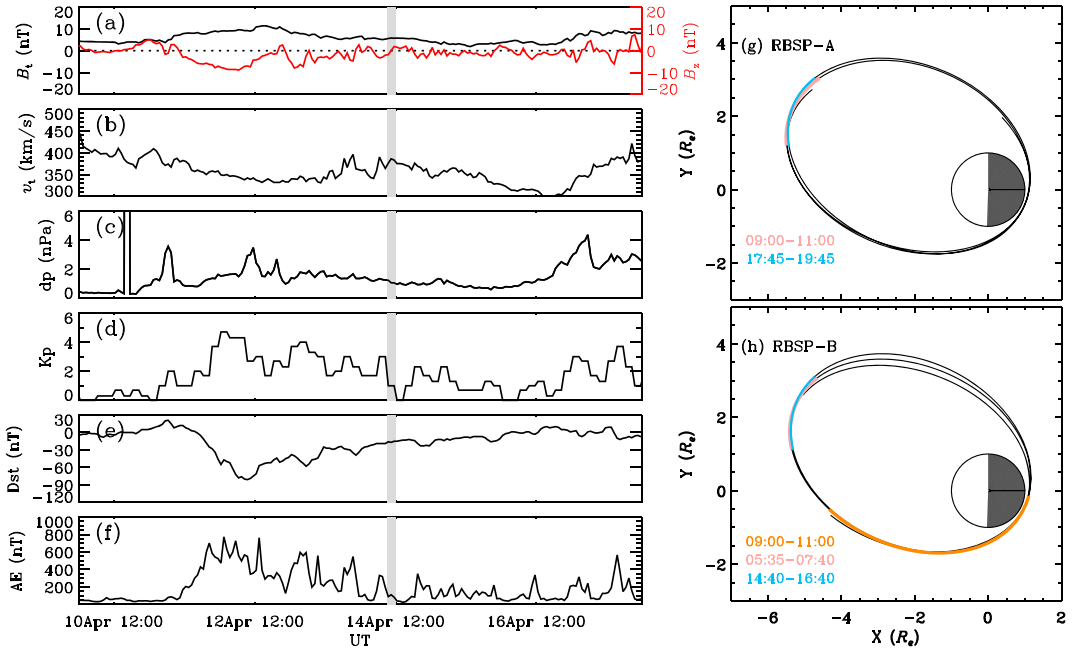

Figure 1. Interplanetary parameters and geomagnetic indices. The gray region indicates magnetosonic wave event, which occurred during the recovery phase of a geomagnetic storm. (a) Magnetic intensity (black solid line) and B_z component (red solid line) in geocentric solar magnetospheric coordinates, (b) solar wind velocity, (c) dynamical pressure of solar wind, (d) Kp index, (e) Dst index, (f) AE index, and (g and h) the orbits of Van Allen Probe A and B on 14 April 2014 projected in the X-Y plane of solar magnetic coordinate system. The red and orange lines in panels (g) and (h) indicate the intervals 09:00–11:00 UT when magnetosonic waves were observed and the blue lines represent the intervals when probes A and B passed the similar magnetic local time region with magnetosonic event.

2. Observations and Analysis

Figures 1a–1f show the interplanetary parameters and geomagnetic indices during the period 10–18 April 2014 obtained from CDAweb-OMNI database. A moderate geomagnetic storm occurred from 11 April 2014 probably resulting from the appearance of southern interplanetary magnetic field. During this storm interval, several substorm activities with increasing AE indices were also observed. In this study, we primarily focus on the interval 09:00–11:00 UT on 14 April 2014 when Van Allen Probe A (Mauk et al., 2013) measured a discrete MS waves event, which we will describe below. This interval was during the late recovery phase of the moderate geomagnetic storm with the small values of the AE index and the slow increasing of Dst. Figures 1g and 1h present the orbits of Van Allen Probes A and B projected in the X-Y plane of solar magnetic coordinate system on 14 April 2014, respectively. The orange line in Figure 1g and red line in Figure 1h indicate the time interval 09:00–11:00 UT. During this period only Van Allen Probe A observed MS waves. This suggests that the occurrence of the waves is spatially localized. The red and blue lines in these figures show the orbits of Probe A (blue) and Probe B (red) when they covered the same magnetic local time. Again Probe A observed MS while Probe B, crossing this region 5 hr later, did not. This would indicate that the waves have a short lifetime.

Figure 2 presents the overview of electromagnetic waves, plasma, electric, and magnetic fields measurement for MS wave event captured by Van Allen Probe A. Figures 2a and 2b show the components of magnetic and electric field fluctuation in magnetic field-aligned (MFA) coordinates. We use level-3 magnetic field data with 1-s time resolution in the geocentric solar ecliptic (GSE) coordinate system recorded by the onboard magnetometer, part of the Electric and Magnetic Field Instrument Suite and Integrated Science suite (Kletzing et al., 2013), to produce the detrended magnetic fluctuations. Then we transform the magnetic data in GSE coordinates into MFA coordinates (Takahashi et al., 2015, 2018). The field-aligned (or compressional) direction in the MFA coordinate system is determined by the 500-s running average of the magnetic field, the azimuthal direction is obtained by the cross product of the field-aligned vector and satellite position vector, and the radial direction completes the triad. This coordinate system helps us understand the ULF wave properties since the radial, azimuthal, and field-aligned components of magnetic field in MFA

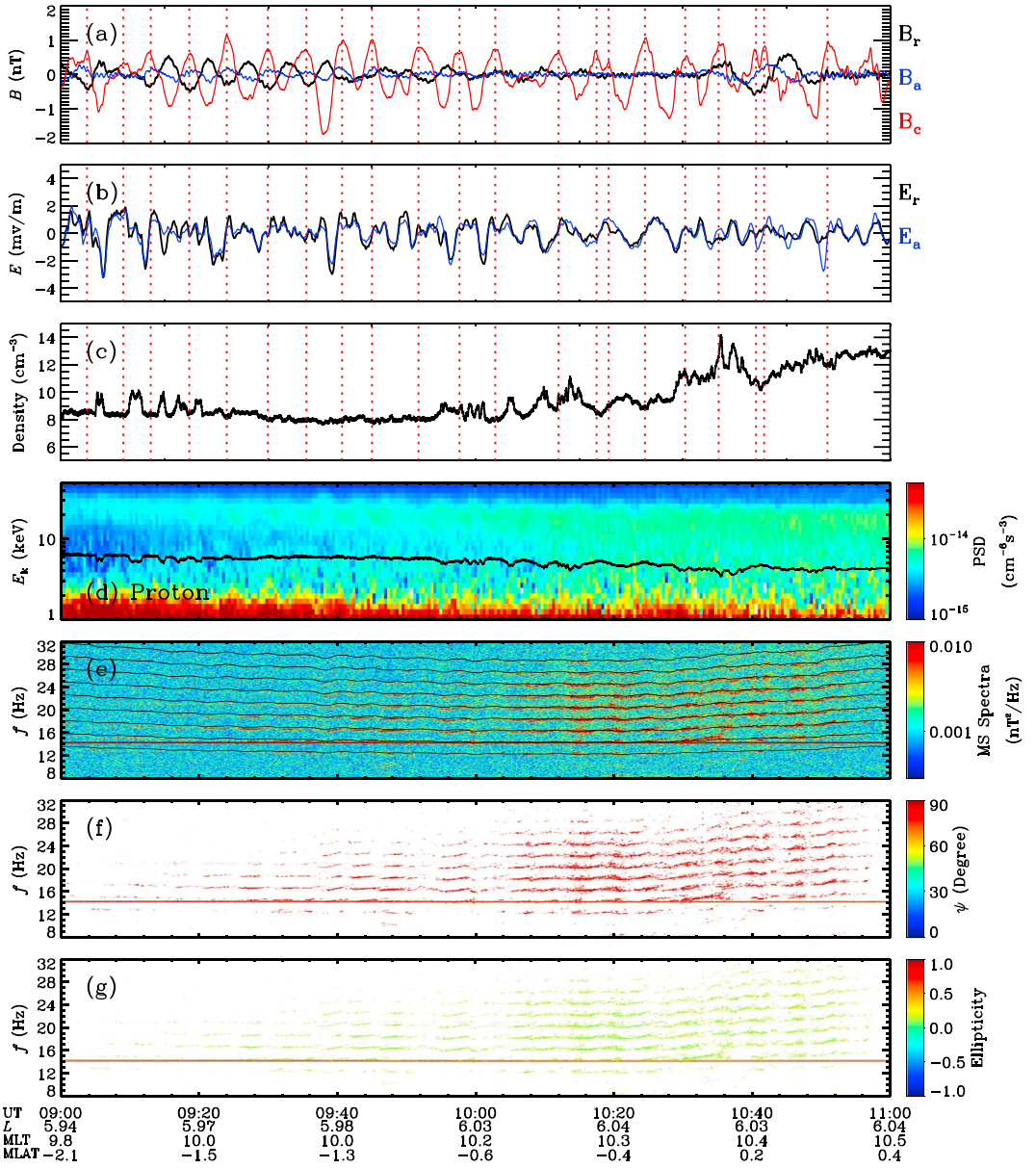

Figure 2. (a) Detrended magnetic field components in magnetic field-aligned coordinates, (b) electric field components in magnetic field-aligned coordinates, (c) electron number density derived from potential, (d) phase space densities of protons at 90° pitch angle recorded by Helium, Oxygen, Proton, and Electron, (e) magnetic power spectral density based on the measurement of Electric and Magnetic Field Instrument Suite and Integrated Science magnetometer, (f) normal angle, and (g) the ellipticity of magnetic field polarization. The red dotted lines in panels (a)–(c) are selected as the peaks of compressional components of magnetic field. The black solid line in panel (d) represents the Alfvenic energy. The solid lines in panel (e) represent the multiples of the local proton gyrofrequency from $6f_{cp}$ to $14f_{cp}$. The red horizontal lines near 14 Hz in panels (e)–(g) are not magnetosonic wave activity. They are probably noise. MS = magnetosonic; PSD = phase space density.

(denoted B_r, B_a, and B_c, respectively) correspond to the poloidal, toroidal Alfvenic waves, and compressional wave, respectively. Finally, the magnetic field measurements themselves were averaged over 22 s to suppress spin modulation. The background field was determined using 500-s averages of the data, and the detrended magnetic fields are the difference between the two. Similarly, the detrended electric fields are obtained from the level-3 electric field with 10.9-s time resolution in modified GSE coordinates measured by the Electric Field and Waves Suite (EFW) instruments (Wygant et al., 2013). We transform the electric data from modified GSE to GSE coordinates and then to MFA coordinate system. Note that the spin-axis-aligned

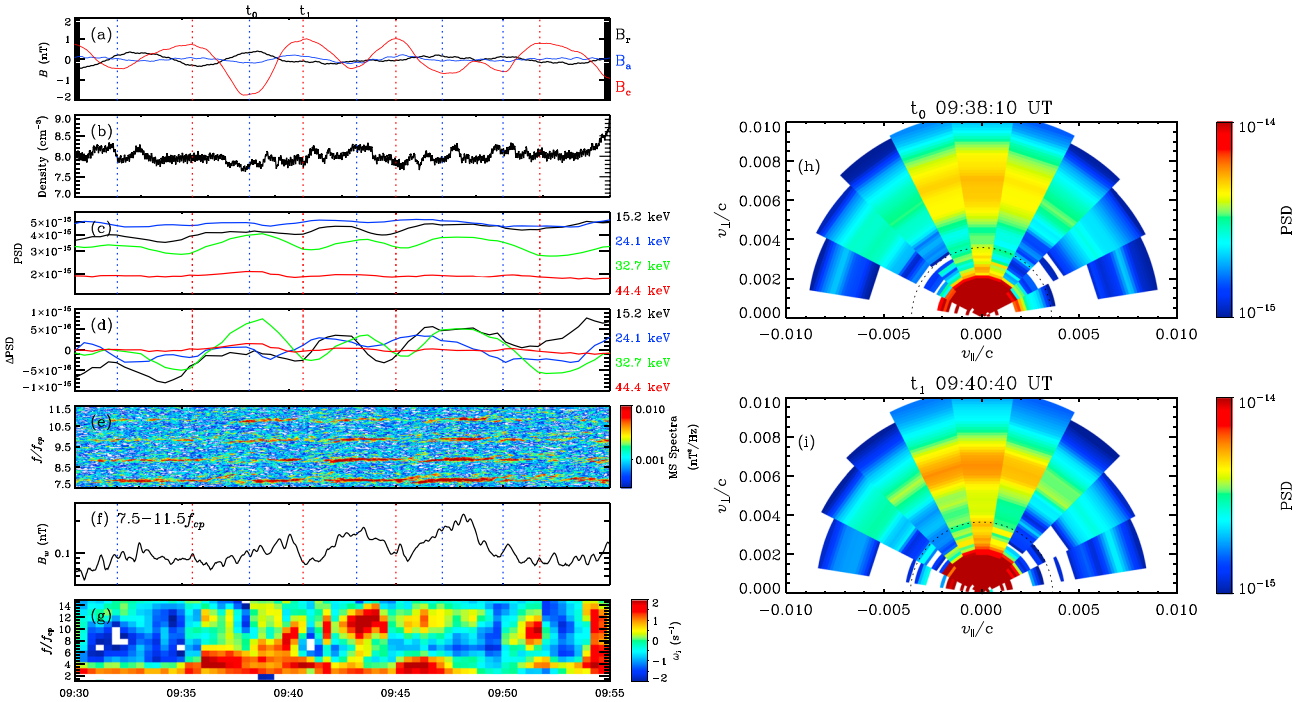

Figure 3. (a) Detrended magnetic field components in magnetic field-aligned coordinates; (b) electron number density; (c) proton PSDs at 90° pitch angle at four energies; (d) the detrended proton PSD at 90° pitch angle at four different energies, 15.2, 24.1, 32.7, and 44.4 keV; (e) magnetic power spectral density as functions of time and normalized frequency to the local proton gyrofrequency f_{cp}; (f) root-mean-square wave amplitude integrating from $7.5f_{cp}$ to $11.5f_{cp}$; (g) the calculated growth rate based on linear theory; and (h and i) proton PSDs as functions of $v_{\parallel}$ and $v_{\perp}$ at t_0 and t_1. The red and blue dotted lines in panels (a)–(d) and (f) are selected as the peaks and valleys of compressional components of magnetic field, respectively. The black dotted lines in panels (h) and (i) represent the Alfvenic velocity. Note that the background magnetic intensity between 09:30 to 09:55 UT was between 134 and 140 nT. MS = magnetosonic; PSD = phase space density.

component of electric field is obtained by the assumption $E \cdot B = 0$. The detrended electric fields are the difference between 22-s running averaged fields and 500-s running averaged fields. Figure 2a shows that ULF waves were clearly present during 09:00–11:00 UT with time period of ~9 min and with compressional component of magnetic field dominant over the poloidal and toroidal components. The red dashed lines mark the peaks of fluctuating compressional magnetic field. The corresponding detrended electric fields (Figure 2b) in radial and azimuthal directions show the fluctuations of comparable periodicity and presented roughly in-phase variation, indicating linear polarization. Electron number density is derived from the spacecraft potential measured by EFW instrument and shown in Figure 2c. The low values of plasma density (~10 cm^{-3}) denotes that Van Allen Probe A located outside the plasmapause. Though the density profile exhibits moderate variation, the correlation between plasma density and magnetic fluctuations were not obvious. Figure 2d presents proton phase space density (PSD) at pitch angle 90° obtained from the 22-s cadence measurement of the Helium, Oxygen, Proton, and Electron Mass Spectrometer (Funsten et al., 2013). Over the entire interval of interest, proton PSD at 90° presents a ring-like distribution, that is, a PSD peak around 10–20 keV. This ring distribution could provide free energy to generate MS waves. Due to the variations of number density and background magnetic field the profile of Alfvenic energy also presented the variation out phase of density variation. The Alfvenic energy basically fluctuated at the energy range 4–7 keV, which is lower than the energy of proton ring distribution. The proximity of proton ring energy and Alfvenic energy favors the excitation of MS waves (Chen et al., 2010). The ratios of ring velocity to Alfvenic velocity were 1.8 to 2.2, consistent with Chen et al. (2010). The relatively smooth proton PSD excludes the occurrence of proton injection and in contrast the periodic modulation of proton at high energy (>1 keV) is attributed to ULF waves, which will be investigated in the context. Figures 2e–2g show the magnetic power spectral density, wave normal angle (the angle between wave vector and background magnetic field), and the ellipticity of magnetic field polarization over the frequency range of 0–32 Hz. We use high-resolution level-3 magnetic field data with 64 samples per second, which is transformed into MFA coordinate system. Then 2,048 points 93.75% overlapping fast Fourier transform is adopted to obtained the power spectral den-

sity and singular value decomposition method (Santolík et al., 2003) is adopted to obtain the corresponding wave normal angle and ellipticity. During the interval the spacecraft was very close to the magnetic equator (within ~2°). The obtained wave spectra (Figure 2e) show discrete harmonics with each harmonic close to the multiples of the local proton gyrofrequency (the solid lines). The waves have near-perpendicular wave normal angle (>85°) and linear polarization (~0). Those features strongly support that these observed waves are equatorial MS waves in the source region. Even more remarkable is that the discrete frequencies of MS waves also closely follow the fluctuating proton gyrofrequency and its harmonics, due to the ULF wave activity. Such fine-scale modulation in discrete wave frequency by the ULF waves has never been reported before. To reveal the nature of ULF modulation of MS waves, we examine the observations in two following intervals, 09:30–09:55 and 10:25–10:55 UT, in detail below.

Figure 3 presents the detailed observations during 09:30–09:55 UT. Figure 3a, similar to Figure 2a, shows that the compressional component of the detrended magnetic fields dominates over the other two components. The peaks and valleys of compressional magnetic fluctuation are marked by the red and blue vertical dashed lines, respectively. The electron density profile was relatively constant (Figure 3b). The PSDs at 24.1 keV were larger than those at 16.2 keV and the PSDs at 32.7 keV, which supports the presence of proton ring distribution of the ring energy near 24.1 keV. Such ring distribution may provide the free energy for MS waves (Chen et al., 2010, 2011). The proton PSDs of 90° pitch angle (Figure 3c), particularly at 32.7 keV, show the variation out of phase with the compressional component of magnetic field. Slight phase shift at different energies is also noted in Figure 3d, where the detrended PSDs are plotted. For each energy, the detrended PSDs were calculated by subtracting the mean value of PSD over the 25-min interval. In addition to the energy-dependence phase shift, the amplitude of the PSD fluctuations induced by ULF waves are energy dependent; the amplitude at 24.1 keV is smaller than those at 15.2 and 32.7 keV. No appreciable variation is seen at 44 keV. The dependence of the phase shift relative to the ULF waves and the amplitude of PSD variations on energy yield the variation of ring distribution and thus the variation of the free energy to excite MS waves. It should be noted that the MS wave growth rate depends on not only proton distribution but also ambient plasma and background magnetic field (Chen et al., 2010). For the selected 25-min interval, relative variation of both magnetic field and plasma density is low, and thus, the variation of proton distribution primarily influences the generation of MS waves, which will be shown below. Figure 3e shows PSD of magnetic field for MS waves as functions of time and normalized frequency to the local proton gyrofrequency f_{cp} within the range $7f_{cp}$–$11.5f_{cp}$ (16–24 Hz). The corresponding root-mean-square wave amplitude integrating over the frequency range from $7.5f_{cp}$ to $11.5f_{cp}$ is shown in Figure 3f. One can see that the variation of MS waves shows similar periodicity to ULF wave field (comparing Figures 3a and 3f). The intensity of MS waves tended to intensify at the minima (sometimes with small offset) of magnetic compressional component fluctuations, which is corresponding to enhanced proton PSD. This correspondence with proton PSD enhancement is expected from linear theory (Chen et al., 2010). The small offset from the maxima of proton PSD is likely caused by the perpendicular propagation of MS waves. Figure 3g shows the growth rate at normal angle 89.5° and for integral harmonics, calculated using linear growth rate formula (Chen, 2015). For the calculation, the proton distribution at 90° pitch angle is provided by the Helium, Oxygen, Proton, and Electron measurement, and background electron number density is derived from EFW detection. The calculated growth rates also present similar temporal variation to proton PSD variation. Comparison between linear growth rate (Figure 3g) and wave amplitude (Figure 3f) shows that enhanced wave amplitude corresponds to enhanced positive growth rate (wave growth), that wave amplitude tends to be weakened at negative growth rate (wave damping). The consistency supports that the variation of MS waves is modulated by the variation of proton ring distribution, which is regulated by the ULF wave phase. Such detailed analysis directly confirms the role of ring current proton variation in the excitation of MS waves in the source region. In addition, there is weak discrepancy between calculated growth rate and observed MS wave amplitude. For example, during 09:30 to 09:35 UT the growth rates above $5f_{cp}$ are negative, while the observed MS wave amplitude was about 0.1 nT. Such discrepancy probably results from the uncertainty of electron number density, which is empirically derived from spacecraft potential, and the perpendicular propagation of MS waves. The perpendicular propagation allows MS waves propagate across field lines and ULF wave structures (including density structures). As a consequence, the observation of ULF-modulated MS waves is rather rare, which makes the event under our study a fortunate one. Figures 3h and 3i show two examples of PSD distributions as functions of $v_{\parallel}$ and $v_{\perp}$ at 09:38:10 and 09:40:40 UT, which correspond to the minimum and maximum of the fluctuating magnetic field compressional component, respectively. Ring-like

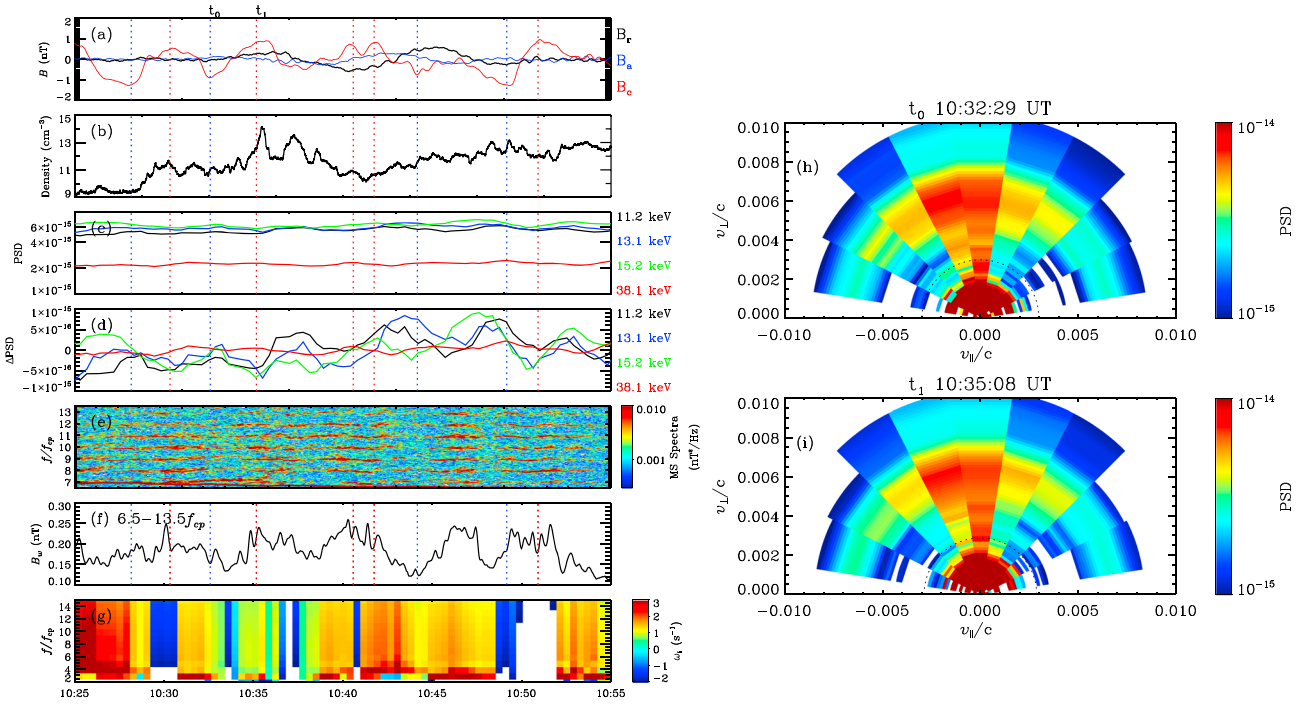

Figure 4. (a) Detrended magnetic field components in magnetic field-aligned coordinates; (b) electron number density; (c) proton PSDs at four energies; (d) the detrended proton PSD at four energies; (e) magnetic power spectral density as functions of time and normalized frequency to the local proton gyrofrequency f_{cp}; (f) root-mean-square wave amplitude integrating from $6.5f_{cp}$ to $13.5f_{cp}$; (g) the calculated growth rate based on linear theory; and (h and i) proton PSDs as functions of $v_{\|}$ and $v_{\perp}$ at t_0 and t_1. The red and blue dotted lines in panels (a)–(d) and (f) are selected as the peaks and valleys of compressional components of magnetic field, respectively. The black dotted lines in panels (h) and (i) represent the Alfvenic velocity. Note that the background magnetic intensity between 10:25 and 10:55 UT was between 134 and 147 nT. MS = magnetosonic; PSD = phase space density.

distributions (that is, the presence of a maximum along $v_{\perp}$ direction) are evident at both times, with ring energy close to Alfven energy (denoted by dashed line). The peak PSD is clearly enhanced at the later time, leading to enhancement in the wave growth rate. This is the first evidence of ULF wave modulation of ring distribution and free energy for MS waves.

Figure 4, in the same format as Figure 3, shows the observation during another interval from 10:25 to 10:55 UT. Both the ULF wave activities and proton PSDs show the similar relation as mentioned above. During this interval the compressional component fluctuations of ULF waves were dominated except near 10:45 UT when the radial component fluctuation is comparable with that for compressional component. MS waves also exhibit intensity variation at a temporal rate close to the period of the ULF wave, and the calculated growth rate exhibits alternation between positive and negative values, suggesting the turning on/off of the free energy of the MS waves. However, the one-to-one correspondence between the minima of ULF wave compressional component (or maxima of PSD variation at 90° pitch angle) and MS wave intensity peaks is not evident in Figure 4 (in comparison with Figure 3). One reason for the lack of the correspondence is that for this interval electron densities vary substantially, leading to the variation of Alfvenic energy and thus affecting the growth rate. Another reason for complicating the relation between ULF wave and MS wave intensity is that the waves are propagating perpendicularly across the field lines, which smooths out the phase relation between MS wave intensity and the ULF wave.

In order to better show the correlation between ULF waves and proton PSD and thus MS wave intensity, the scatter plot of B_c fluctuation versus proton PSD variation and MS wave amplitude for two intervals 09:30–09:55 and 10:25–10:55 UT are presented in Figure 5. Figure 5a shows the B_c fluctuation of ULF waves versus PSD variation at energy 32.7 keV. Their correlation coefficient is −0.75, confirming the strong and negative correlation between ULF waves and proton PSD. The correlation coefficients at other energies 15.2, 24.1, and 44.4 keV are −0.51, −0.04, and −0.75, respectively. Such different correlations at different energies are probably due to the energy-dependent response of protons to ULF waves. Figure 5b presents B_c fluctuation versus the MS wave amplitude integrated from $7.5f_{cp}$ to $11.5f_{cp}$. Because of the perpendicular

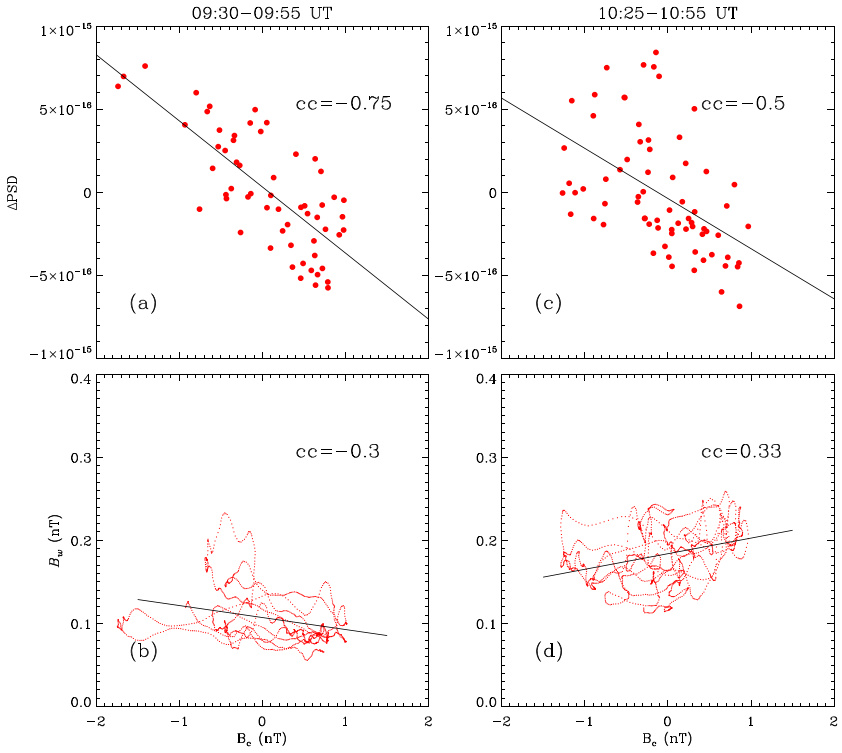

Figure 5. Scatter plot of the fluctuation of compressional magnetic field versus delta PSD (a, c) and magnetosonic wave amplitude (b, d) during two intervals (a and b, and c and d). The solid lines represent the linear regression results. cc means the corresponding correlation coefficient. PSD = phase space density.

propagation of MS waves the correlation between ULF and MS waves (correlation coefficient −0.33) is not significant as that between ULF waves and proton PSD. The correlation coefficient −0.33 suggests the weak correlation between ULF waves and MS waves. Figure 5c is similar to Figure 5a but at energy 13.1 keV during 10:25 to 10:55 UT. The results that the cross correlation between ULF waves and proton PSD is still moderate with correlation coefficient −0.5. The correlation coefficients at other energies 11.2, 15.2, and 38.2 keV are −0.28, −0.38, and −0.12, respectively. However, the unexpected positive cross correlation occurs between ULF waves and MS wave amplitude shown in Figure 5d. Such poor correlation is due to the significant variation of electron number density, which complicates the MS generation process, and the perpendicular propagation of MS waves. As we mentioned above, the perpendicular propagation allows MS waves propagate across field lines and ULF wave structures (including density structures). Hence, the observation of the ULF wave modulation of MS waves is rather rare, which makes the event under our study a fortunate one.

3. Conclusions and Discussions

In this study, we report a MS wave event accompanying with ULF fluctuations. We use Van Allen Probes waves and plasma data to reveal the relationship among ULF waves, proton distribution, and MS waves and perform linear analysis using the observed proton distribution. The principal conclusions are summarized as follows:

1. ULF waves significantly modulated the energetic proton ring distribution and therefore free energy available for MS waves.
2. The spectra and intensities of MS waves modulated by compressional ULF waves are reported for the first time.
3. The modulation of MS waves by ULF waves can be accounted for by linear theory and MS wave propagation.

As we discussed above, the compressional ULF waves modulated the energetic proton distribution resulting in changes in the intensity of the MS waves. It is expected from linear theory that when plasma density and background magnetic field variation are small, the peaks of MS intensity should match the peaks of proton

ring PSD. However, the observation shows that the peaks of MS wave intensity sometimes are subject to small separation from the proton PSD peak. This is likely due to perpendicular propagation of MS waves across field lines and density structures, which tends to smooth out the relation between MS waves and ULF wave phase. As a result, the observation of MS waves modulated by ULF wave is less evident and relatively rare, compared with the observation of chorus waves modulated by ULF waves (Li et al., 2011; Xia et al., 2016). Chorus waves tend to propagate along the field line, and thus, the phase relation between chorus wave intensity and ULF waves can be well maintained. Nonetheless, the rare and fortunate observation of MS waves modulated by ULF waves provides strong support for the proton ring as free energy for MS wave excitation.

MS wave event in this study appeared as discrete band at the nearly exact multiple harmonics of local gyrofrequency. Its temporal variation can be discrete or continuous, which is subject to the ULF wave modulation on proton PSD distribution and the variation of cold electron number density. Moreover, the temporal variation of MS wave power at all frequencies performed simultaneously, showing no dispersive feature. In contrast, previous studies (Boardsen et al., 2014; Fu et al., 2014; Němec et al., 2015; Walker et al., 2016) investigated the occurrence of periodic rising tone MS wave. Such MS waves consist of multiple periodic repetitions with gap ~180 s, and each repetition presents as rising tone (dispersive) with sweep rate ~1 Hz/s. In order to explain such feature, which is a still open question, several potential mechanisms have been proposed including nonlinear wave particle interaction, dispersive propagation effect, ULF wave modulation, and cold electron density modulation. The MS event in this study is essentially different from such periodic rising tone events, which gives insight into the coupling between ULF waves and very low frequency waves.

Acknowledgments
The authors used geomagnetic indices provided by OMNIWeb (http://omniweb.gsfc.nasa.gov/form/dx1.html). The Van Allen Probes data are available at the websites (http://emfisis.physics.uiowa.edu/Flight/ for EMFISIS). This research was supported by the NSF grants AGS-1203747 and AGS-1405041 and NASA grants NNX13AE34G, NNX10AK99, NNX15AF55G, and 80NSSC18K1034.

References

Balikhin, M. A., Shprits, Y. Y., Walker, S. N., Chen, L., Cornilleau-Wehrlin, N., Dandouras, I., et al. (2015). Observations of discrete harmonics emerging from equatorial noise. *Nature Communications*, *6*, 7703. https://doi.org/10.1038/ncomms8703

Boardsen, S. A., Gallagher, D. L., Gurnett, D. A., Peterson, W. K., & Green, J. L. (1992). Funnel-shaped, low-frequency equatorial waves. *Journal of Geophysical Research*, *97*(A10), 14,967–14,976. https://doi.org/10.1029/92JA00827

Boardsen, S. A., Hospodarsky, G. B., Kletzing, C. A., Pfaff, R. F., Kurth, W. S., Wygant, J. R., & MacDonald, E. A. (2014). Van Allen Probe observations of periodic rising frequencies of the fast magnetosonic mode. *Geophysical Research Letters*, *41*, 8161–8168. https://doi.org/10.1002/2014GL062020

Bortnik, J., & Thorne, R. M. (2010). Transit time scattering of energetic electrons due to equatorially confined magnetosonic waves. *Journal of Geophysical Research*, *115*, A07213. https://doi.org/10.1029/2010JA015283

Chen, L. (2015). Wave normal angle and frequency characteristics of magnetosonic wave linear instability. *Geophysical Research Letters*, *42*, 4709–4715. https://doi.org/10.1002/2015GL064237

Chen, L., Maldonado, A., Bortnik, J., Thorne, R. M., Li, J., Dai, L., & Zhan, X. (2015). Nonlinear bounce resonances between magnetosonic waves and equatorially mirroring electrons. *Journal of Geophysical Research: Space Physics*, *120*, 6514–6527. https://doi.org/10.1002/2015JA021174

Chen, L., Thorne, R. M., Jordanova, V. K., & Horne, R. B. (2010). Global simulation of magnetosonic wave instability in the storm time magnetosphere. *Journal of Geophysical Research*, *115*, A11222. https://doi.org/10.1029/2010JA015707

Chen, L., Thorne, R. M., Jordanova, V. K., Thomsen, M. F., & Horne, R. B. (2011). Magnetosonic wave instability analysis for proton ring distributions observed by the LANL magnetospheric plasma analyzer. *Journal of Geophysical Research*, *116*, A03223. https://doi.org/10.1029/2010JA016068

Curtis, S., & Wu, C. (1979). Gyroharmonic emissions induced by energetic ions in the equatorial plasmasphere. *Journal of Geophysical Research*, *84*(A6), 2597–2607. https://doi.org/10.1029/JA084iA06p02597

Elkington, S. R., Hudson, M. K., & Chan, A. A. (1999). Acceleration of relativistic electrons via drift-resonant interaction with toroidal-mode Pc-5 ULF oscillations. *Geophysical Research Letters*, *26*, 3273–3276. https://doi.org/10.1029/1999GL003659

Fälthammar, C.-G. (1965). Effects of time-dependent electric fields on geomagnetically trapped radiation. *Journal of Geophysical Research*, *70*, 2503–2516. https://doi.org/10.1029/JZ070i011p02503

Fu, H. S., Cao, J. B., Zhima, Z., Khotyaintsev, Y. V., Angelopoulos, V., Santolík, O., et al. (2014). First observation of rising-tone magnetosonic waves. *Geophysical Research Letters*, *41*, 7419–7426. https://doi.org/10.1002/2014GL061867

Funsten, H. O., Skoug, R. M., Guthrie, A. A., MacDonald, E. A., Baldonado, J. R., Harper, R. W., et al. (2013). Helium, Oxygen, Proton, and Electron (HOPE) mass spectrometer for the Radiation Belt Storm Probes mission. *Space Science Reviews*, *179*, 423–484. https://doi.org/10.1007/s11214-013-9968-7

Gurnett, D. A. (1976). Plasma wave interactions with energetic ions near the magnetic equator. *Journal of Geophysical Research*, *81*, 2765–2770. https://doi.org/10.1029/JA081i016p02765

Horne, R. B., Thorne, R. M., Glauert, S. A., Meredith, N. P., Pokhotelov, D., & Santolík, O. (2007). Electron acceleration in the Van Allen radiation belts by fast magnetosonic waves. *Geophysical Research Letters*, *34*, L17107. https://doi.org/10.1029/2007GL030267

Horne, R. B., Wheeler, G. V., & Alleyne, H. S. C. K. (2000). Proton and electron heating by radially propagating fast magnetosonic waves. *Journal of Geophysical Research*, *105*(A12), 27,597–27,610. https://doi.org/10.1029/2000JA000018

Hughes, W. J. (1994). Magnetospheric ULF waves: A tutorial with a historical perspective. *Washington DC American Geophysical Union Geophysical Monograph Series*, *81*, 1–11. https://doi.org/10.1029/GM081p0001

Kletzing, C. A., Kurth, W. S., Acuna, M., MacDowall, R. J., Torbert, R. B., Averkamp, T., et al. (2013). The Electric and Magnetic Field Instrument Suite and Integrated Science (EMFISIS) on RBSP. *Space Science Reviews*, *179*, 127–181. https://doi.org/10.1007/s11214-013-9993-6

Li, J., Ni, B., Xie, L., Pu, Z., Bortnik, J., Thorne, R. M., et al. (2014). Interactions between magnetosonic waves and radiation belt electrons: Comparisons of quasilinear calculations with test particle simulations. *Geophysical Research Letters*, *41*, 4828–4834. https://doi.org/10.1002/2014GL060461

Li, X., Tao, X., Lu, Q., & Dai, L. (2015). Bounce resonance diffusion coefficients for spatially confined waves. *Geophysical Research Letters*, *42*, 9591–9599. https://doi.org/10.1002/2015GL066324

Li, W., Thorne, R. M., Bortnik, J., Nishimura, Y., & Angelopoulos, V. (2011). Modulation of whistler mode chorus waves: 1. Role of compressional Pc4-5 pulsations. *Journal of Geophysical Research*, *116*, A06205. https://doi.org/10.1029/2010JA016312

Liu, K., Gary, S. P., & Winske, D. (2011). Excitation of magnetosonic waves in the terrestrial magnetosphere: Particle-in-cell simulations. *Journal of Geophysical Research*, *116*, A07212. https://doi.org/10.1029/2010JA016372

Liu, N., Su, Z., Zheng, H., Wang, Y., & Wang, S. (2018). Prompt disappearance and emergence of radiation belt magnetosonic waves induced by solar wind dynamic pressure variations. *Geophysical Research Letters*, *45*, 585–594. https://doi.org/10.1002/2017GL076382

Ma, Q., Li, W., Chen, L., Thorne, R. M., & Angelopoulos, V. (2014). Magnetosonic wave excitation by ion ring distributions in the Earth's inner magnetosphere. *Journal of Geophysical Research: Space Physics*, *119*, 844–852. https://doi.org/10.1002/2013JA019591

Ma, Q., Li, W., Thorne, R. M., Bortnik, J., Kletzing, C. A., Kurth, W. S., & Hospodarsky, G. B. (2016). Electron scattering by magnetosonic waves in the inner magnetosphere. *Journal of Geophysical Research: Space Physics*, *121*, 274–285. https://doi.org/10.1002/2015JA021992

Mauk, B. H., Fox, N. J., Kanekal, S. G., Kessel, R. L., Sibeck, D. G., & Ukhorskiy, A. (2013). Science objectives and rationale for the radiation belt storm probes mission. *Space Science Reviews*, *179*, 3–27. https://doi.org/10.1007/s11214-012-9908-y

Meredith, N. P., Horne, R. B., & Anderson, R. R. (2008). Survey of magnetosonic waves and proton ring distributions in the Earth's inner magnetosphere. *Journal of Geophysical Research*, *113*, A06213. https://doi.org/10.1029/2007JA012975

Němec, F., Santolík, O., Gereová, K., Macúšová, E., de Conchy, Y., & Cornilleau-Wehrlin, N. (2005). Initial results of a survey of equatorial noise emissions observed by the Cluster spacecraft. *Planetary and Space Science*, *53*, 291–298. https://doi.org/10.1016/j.pss.2004.09.055

Němec, F., Santolík, O., Hrbáčková, Z., Pickett, J. S., & Cornilleau-Wehrlin, N. (2015). Equatorial noise emissions with quasiperiodic modulation of wave intensity. *Journal of Geophysical Research: Space Physics*, *120*, 2649–2661. https://doi.org/10.1002/2014JA020816

Perraut, S., Roux, A., Robert, P., Gendrin, R., Sauvaud, J.-A., Bosqued, J.-M., et al. (1982). A systematic study of ULF waves above F_H+ from GEOS 1 and 2 measurements and their relationships with proton ring distributions. *Journal of Geophysical Research*, *87*(A8), 6219–6236. https://doi.org/10.1029/JA087iA08p06219

Russell, C. T., Holzer, R. E., & Smith, E. J. (1970). OGO 3 observations of ELF noise in the magnetosphere. 2. The nature of the equatorial noise. *Journal of Geophysical Research*, *75*, 755–768. https://doi.org/10.1029/JA075i004p00755

Santolík, O., Nemec, F., Gereová, K., Macúšová, E., Conchy, Y., & Cornilleau-Wehrlin, N. (2004). Systematic analysis of equatorial noise below the lower hybrid frequency. *Annales Geophysicae*, *22*, 2587–2595. https://doi.org/10.5194/angeo-22-2587-2004

Santolík, O., Parrot, M., & Lefeuvre, F. (2003). Singular value decomposition methods for wave propagation analysis. *Radio Science*, *38*(1), 1010. https://doi.org/10.1029/2000RS002523

Santolík, O., Pickett, J. S., Gurnett, D. A., Maksimovic, M., & Cornilleau-Wehrlin, N. (2002). Spatiotemporal variability and propagation of equatorial noise observed by Cluster. *Journal of Geophysical Research*, *A12*, 1495. https://doi.org/10.1029/2001JA009159

Shprits, Y. Y., Runov, A., & Ni, B. (2013). Gyro-resonant scattering of radiation belt electrons during the solar minimum by fast magnetosonic waves. *Journal of Geophysical Research: Space Physics*, *118*, 648–652. https://doi.org/10.1002/jgra.50108

Su, Z., Zhu, H., Xiao, F., Zong, Q. G., Zhou, X. Z., Zheng, H., et al. (2015). Ultra-low-frequency wave-driven diffusion of radiation belt relativistic electrons. *Nature Communications*, *6*, 10096. https://doi.org/10.1038/ncomms10096

Takahashi, K., Denton, R. E., Kurth, W., Kletzing, C., Wygant, J., Bonnell, J., et al. (2015). Externally driven plasmaspheric ULF waves observed by the Van Allen Probes. *Journal of Geophysical Research: Space Physics*, *120*, 526–552. https://doi.org/10.1002/2014JA020373

Takahashi, K., Oimatsu, S., Nosé, M., Min, K., Claudepierre, S. G., Chan, A., et al. (2018). Van Allen Probes observations of second harmonic poloidal standing Alfvén waves. *Journal of Geophysical Research: Space Physics*, *123*, 611–637. https://doi.org/10.1002/2017JA024869

Walker, S. N., Demekhov, A. G., Boardsen, S. A., Ganushkina, N. Y., Sibeck, D. G., & Balikhin, M. A. (2016). Cluster observations of non-time continuous magnetosonic waves. *Journal of Geophysical Research: Space Physics*, *121*, 9701–9716. https://doi.org/10.1002/2016JA023287

Wygant, J. R., Bonnell, J. W., Goetz, K., Ergun, R. E., Mozer, F. S., Bale, S. D., et al. (2013). The Electric Field and Waves instruments on the Radiation Belt Storm Probes mission. *Space Science Reviews*, *179*, 183–220. https://doi.org/10.1007/s11214-013-0013-7

Xia, Z., Chen, L., Dai, L., Claudepierre, S. G., Chan, A. A., Soto-Chavez, A. R., & Reeves, G. D. (2016). Modulation of chorus intensity by ULF waves deep in the inner magnetosphere. *Geophysical Research Letters*, *43*, 9444–9452. https://doi.org/10.1002/2016GL070280

Yuan, Z., Yu, X., Huang, S., Wang, D., & Funsten, H. O. (2017). In situ observations of magnetosonic waves modulated by background plasma density. *Geophysical Research Letters*, *44*, 7628–7633. https://doi.org/10.1002/2017GL074681